Thermodynamic geometry of spin-one lattice models.
I. Spin and quadrupolar orders and critical scaling functions in one dimension

Riekshika Sanwari [*] and Anurag Sahay [†]

Department of Physics, National Institute of Technology Patna, Patna 800005, India

State space Riemannian geometry is obtained for the one-dimensional Blume-Emery-Griffiths model and its Blume-Capel and Griffiths model limits, and its (pseudo)critical as well as noncritical parameter regimes are extensively investigated. Two codimension one geometries are obtained by taking suitable hypersurfaces in the three-dimensional state space manifold, and the induced thermal metrics are accordingly interpreted in terms of constrained fluctuations. The three-dimensional scalar curvature and the two two-dimensional curvatures are shown to be consistent with Ruppeiner's conjecture relating the inverse of the singular free energy to the thermodynamic scalar curvature. Moreover, they are found to be in an excellent agreement over a greater part of the noncritical region with the corresponding correlation lengths for the spin and the quadrupolar order parameters. The scaling function for the free energy near the pseudocritical and tricritical points is obtained thermodynamically by using Ruppeiner's conjecture. A connection is made between the sign change in the curvatures and the change in fluctuation patterns of the order parameters. In the accompanying paper we shall analyze the geometry of the spin-one model in its mean field approximation.

I. INTRODUCTION

Thermodynamic geometry (TG), as pioneered by Ruppeiner and other researchers, has been extensively used to probe a wide range of thermodynamic systems including fluids, magnetic systems, and several black hole solutions. Employing a metric based on second moments of thermal fluctuation TG renders a Riemannian geometric structure to the thermodynamic state space of the system [1,2]. The thermodynamic metric quantifies in a coordinate-independent way the classical distinguishability between thermodynamic states, so that the easier it is for two states to fluctuate into each other the shorter the separation between them and vice versa.

TG forges a surprising and remarkable connection between its geometric invariants, which are calculated solely from thermodynamics and the underlying statistical mechanical description of the system. Thus, in an early insight Ruppeiner conjectured that in the vicinity of the critical point the state space scalar curvature R is *equal* to the correlation volume ξ^d up to a constant of order unity. Using hyperscaling [3], this insight could be further refined to an equality of the scalar curvature with the inverse of the critical free energy up to a universal constant κ which depends only on the universal critical exponents,

$$R = \kappa \, \frac{1}{\psi_s}, \tag{1}$$

where the critical Massieu function ψ_s is related to the critical free energy density ϕ_s in the usual way, $\phi = -T\psi$. The above equation, considered as a differential equation for the free en-

ergy, could be profitably used to calculate the scaling function of the singular free energy, thus providing a thermodynamics-based alternative to the more challenging calculation based on renormalization group analysis [4,5]. This geometry-energy equation in the Riemannian state space is a centerpiece of TG and is reminiscent of the Einstein's equation which relates space-time curvature to matter energy distribution. It will therefore be apt to refer to the conjectured equality in Eq. (1) as *the Ruppeiner equation*.

It turns out that the Ruppeiner equation can be thought of as the stronger form of a broader conjecture relating geometry to thermodynamics, one which becomes exact in the limit of the critical point. It will be shown in this work, as also has been shown elsewhere, that the conjecture relating curvature to the correlation volume as

$$R \sim \xi^d \tag{2}$$

(where d is spatial dimension) extends to regions much beyond criticality. We shall refer to it as the weak form of Ruppeiner's conjecture. The weak conjecture has found much use recently in calculating the phase coexistence curves and the Widom lines for fluids and other systems [6–9].

Remarkably, the scalar curvature packs even more information about the underlying statistics of interactions via its signature. Thus, it is commonly believed that a positive sign (in the convention used in [1]) of R is indicative of statistically repulsive interactions, while a negative sign is suggestive of statistically attractive interactions [9–15]. For example, the scalar curvature has always been seen to diverge to negative infinity at criticality. However, the issue of signature of R is nuanced as suggested recently in [16], and it still awaits a more fundamental resolution. In addition, scalar curvature in three-dimensional or higher dimensional parameter space has been investigated for only a handful of thermodynamic

[*]riekshikas.phd19.ph@nitp.ac.in
[†]anuragsahay@nitp.ac.in

systems [16–18]. It is of interest to pursue the geometry of higher dimensional parameter spaces to see if apart from the scalar curvature the sectional curvatures could also signify underlying physics.

More generally, R is to be understood as a qualified measure of interactions. While its behavior is well understood broadly, a finer understanding of the geometric curvature is still an ongoing work. In light of this it is important to record the behavior of R for a range of thermodynamic systems. In this context, exactly solved models can serve as important testing grounds to verify the conjectures of TG and to further explore the features of R inasmuch as they offer an analytical control over the partition function and also possibly the correlation length. One of the most important such models used to successfully verify TG is the one-dimensional Ising model which has a (pseudo)critical point at zero temperature in zero magnetic field. The scalar curvature earlier worked out numerically in [19] was later found to be a surprisingly simple expression [20]. Some other cases where TG has been applied to exactly solved models are the Ising model on a Bethe lattice [21], the Ising model on planar random graphs [22], the spherical model [23] and the one-dimensional Potts model [24], and a decorated two-parameter Ising spin chain with frustration [25].

An Ising model with lattice spins $S_i = \pm 1$ naturally generalizes to the spin-one model with lattice spins $S_i = 0, \pm 1$. What might seem like an innocuous addition of a degree of freedom to the lattice sites results in a rich and varied phase structure of the spin-one model. This is because in addition to the Ising-model-like interactions, the spin-one model admits the possibility of a nontrivial biquadratic coupling of quadrupoles S_i^2 to each other and their interaction with an ordering field independent of the magnetic field. In effect, the thermodynamics of a spin-one model is governed by two order parameters, the spin $\langle S_i \rangle$ and the quadrupole moment $\langle S_i^2 \rangle$. Both the order parameters, while kinematically coupled, are separate stochastic variables and their interplay leads to a rich phase structure with coexistence surfaces bordered by critical lines and coexistence lines which meet in one or more tricritical points.

Naturally, therefore, spin-one lattice models have been extensively used to model the behavior of interacting systems with two types of ordering processes. One of the most popular spin-one models, the Blume-Emery-Griffiths (BEG) model originally formulated to study the phase behavior He^3-He^4 mixtures, has been widely used to model diverse phenomena. As a model for the phase behavior in Helium mixture it successfully captures the phenomena of superfluid ordering as well as phase separation depending on the relative concentration of the He^3 impurity [26]. In addition, the BEG model has been used in the context of simple fluids to model condensation and solidification [27], in binary alloys to model ferromagnetism and phase separation [28], and in microemulsions [29], to name a few. In the limit of zero biquadratic coupling, known as the Blume-Capel (BC) model [30,31], it has been used to model phase behavior in magnetic systems wherein depending on the strength of crystal field splitting the transition between a paramagnet and a magnetically ordered state changes from first order to second order.

In this work we initiate the study of TG for classical higher spin lattice models beginning with an investigation of the one-dimensional spin-one models, namely, the Blume-Emery-Griffiths model and its limiting cases of the BC model and the Griffiths model [32], where in the latter case the quadratic spin coupling is set to zero. In addition to the advantage of being exactly solved, the one-dimensional spin-one models retain much of the rich phase behavior of their higher dimensional counterparts. Thus, these models continue to display a locus of pseudocritical points, a pseudotricritical point and zero temperature phase coexistence, much of which is amenable to a geometric treatment. Besides, the parameter space of BEG models is three-dimensional, which provides an avenue to explore higher dimensional scalar curvature and various sectional curvatures. In addition, the fact that there are two order parameters in the model gives rise to the possibility of two correlation lengths for some parameter values, and it would be worthwhile exploring if geometry encodes different correlation lengths. In this work we hope to make good use of the given opportunity. In our subsequent work (paper II) we investigate the geometry of criticality and coexistence for the mean field spin-one model [33].

This paper is organized as follows. In Sec. II we obtain the transfer matrix starting with the Hamiltonian of the one-dimensional spin-one model and briefly review its zero temperature phase diagram. In Sec. III we outline our method for obtaining induced thermodynamic geometries from the ambient metric and then argue our case for the two hypersurface geometries we believe are most relevant to our model. Section IV presents a thermodynamic calculation of the scaling form of the singular free energy, including the spin scaling functions, and we make a connection with the Ruppeiner equation. In Sec. V we report our results for the geometry of the one-dimensional BEG model and undertake a detailed survey in different parameter regimes. In Sec. VI we obtain the singular free energy and the geometry of the Griffiths model, and finally in the concluding Sec. VII we summarize our key results, underline some limitations, and try to define the scope of our work.

II. THE ONE-DIMENSIONAL SPIN-ONE MODEL

The most general Hamiltonian of a reflection symmetric spin-one chain of N atoms with nearest-neighbor interaction is

$$\mathcal{H} = -J \sum_i^N S_i S_{i+1} - K \sum_i^N S_i^2 S_{i+1}^2 - H \sum_i^N S_i + D \sum_i^N S_i^2.$$
(3)

The lattice spin variable S_i is Ising like and can take values $+1, -1,$ and 0. In addition to the bilinear coupling terms of strength J and a magnetic field H that couples to the magnetic moment, the Hamiltonian contains a biquadratic coupling term of strength K and a crystal field D which couples to the quadrupole moment. The coupling strengths J and K are positive in the original BEG model [26] with the $K = 0$ limit being the BC model [30,31]. In this report we shall restrict ourselves to the case of nonnegative values of spin exchange and biquadratic exchange, namely, $K, J \geqslant 0$.

The spin-one models have two densities (order parameters), the mean magnetization and the mean quadrupole moment, which in the translationally invariant case are

$$M = \langle S_i \rangle; \ Q = \langle S_i^2 \rangle. \tag{4}$$

The one-dimensional ring of N spins is exactly solvable in the large N limit using the standard transfer matrix technique [34]. The transfer matrix for the Hamiltonian in Eq. (3) is three-dimensional,

$$T = \begin{pmatrix} e^{(-D+H+J+K)\beta} & e^{(H-D)\beta/2} & e^{(-D-J+K)\beta} \\ e^{(H-D)\beta/2} & 1 & e^{-(D+H)\beta/2} \\ e^{(-D-J+K)\beta} & e^{-(D+H)\beta/2} & e^{(-D-H+J+K)\beta} \end{pmatrix}. \tag{5}$$

This gives rise to three eigenvalues in general, $\lambda_1 > \lambda_2 > \lambda_3$. In the limit of infinite N, i.e., the thermodynamic limit, the logarithm of the largest eigenvalue λ_1 becomes the free energy per spin. The free energy (Massieu function) for the zero-field BEG model, $H = 0$, can be obtained in a closed form,

$$\psi = \ln\left[\tfrac{1}{2} e^{-\beta(D+J)} \left(e^{\beta D + \beta J} + e^{2\beta J + \beta K} + e^{\beta K} + \sqrt{W}\right)\right], \tag{6}$$

where

$$\begin{aligned} W = &\left(e^{\beta D + \beta J} + e^{2\beta J + \beta K} + e^{\beta K}\right)^2 \\ &- 4\left(-2e^{\beta D + 2\beta J} + e^{\beta D + \beta J + \beta K} + e^{\beta D + 3\beta J + \beta K}\right). \end{aligned}$$

While there is no finite temperature phase transition for the one-dimensional case, its thermal behavior richly responds to the interplay of various coupling strengths in the Hamiltonian. At the pseudocritical point the eigenvalues λ_1 and λ_2 become asymptotically equal. At the pseudotricritical point all three eigenvalues become asymptotically equal.

The correlation length can be obtained in a standard manner via the ratio of the largest and the next-to-largest eigenvalues. Interestingly, owing to the fact that there are two correlation functions corresponding to the spin-spin and the quadrupole-quadruple correlations, the spin-one model admits the possibility of two separate correlation lengths. Indeed, this possibility is realized for the zero-field BEG model where due to increased symmetry of the transfer matrix there are separate correlation lengths for spin and quadrupole fluctuations, given respectively as

$$\xi_1^{-1} = \log\frac{\lambda_1}{\lambda_2},$$

$$\xi_2^{-1} = \log\frac{\lambda_1}{\lambda_3}. \tag{7}$$

For the nonzero H field there is only one correlation length ξ_1 for correlations in both order parameters [34].

We now discuss the phase structure for the one-dimensional case. Our review closely follows [34], and even Figs. 1 and 2 are exactly the same as those in [34] including the figure labels. In any case the diagrams are easily obtainable from the transfer matrix. Figure 1 shows the phase diagram of the one-dimensional BEG model at $T = 0$. The phase structure of the BC model is very similar. Two phases with $Q = 1$ and $M = \pm 1$ coexist on the a line that is positioned at zero magnetic field. Similarly, two phases $Q = M = 0$ and $Q = M = 1$ or $Q = -M = 1$ coexist on the positive and negative f lines symmetrically placed across the $H = 0$ axis along $\pm H = D - J - K$. There is a discontinuous phase
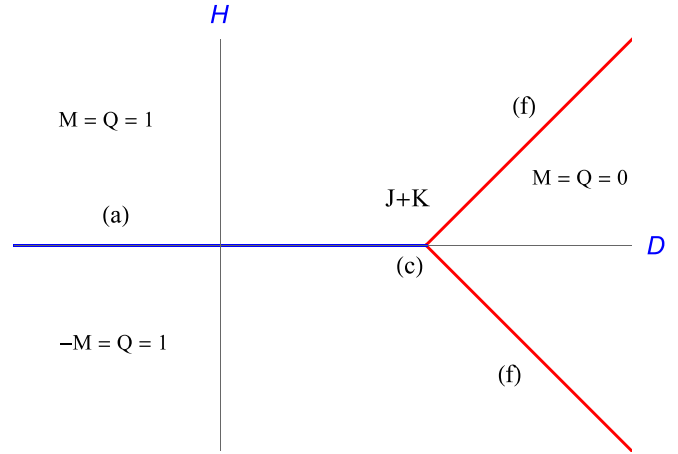

FIG. 1. Zero temperature phase diagram for the spin-one model in the H-D plane with $J > 0$, $J + K > 0$. Two phases coexist on the a line and the f lines in the $T = 0$ plane, and they are a locus of pseudocritical points on approaching from $T > 0$. Point c is a triple point at which three phases coexist in the $T = 0$ plane. On approaching from $T > 0$ it shows pseudotricritical behavior. Adapted from [34].

change on crossing these lines at zero temperature, whereas on approaching these lines from $T > 0$ one sees pseudocritical behavior. The intersection of the a line with the f lines is the triple point c at which three phases coexist. On approaching the c line from $T > 0$ pseudotricritical behavior is seen.

Figure 2 is the zero temperature phase diagram of the one-dimensional Griffiths model, which is the BEG model in the limit of zero quadratic coupling, $J = 0$. On the d line an infinite number of phases coexist in the limit of infinite N. This is because, for $D < K$ on the d line, the $S = 0$ spin is energetically ruled out while the up and down spins are equally likely in the absence of a discriminating quadratic coupling. In other words, the model behaves like a collection of independent
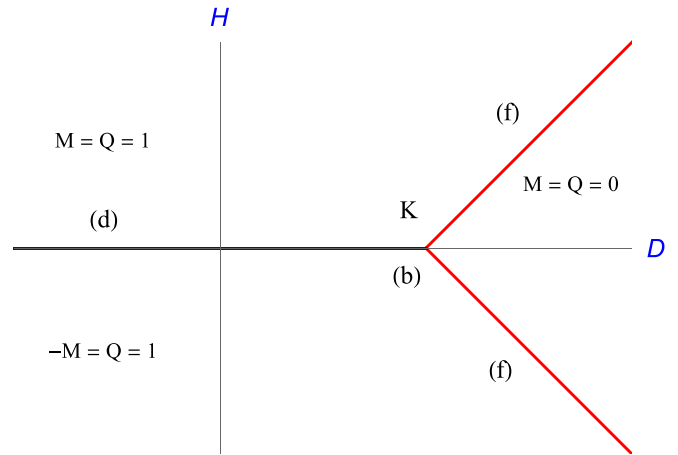

FIG. 2. Zero temperature phase diagram of the spin-one model in the H-D plane with $J = 0$, $K > 0$. Infinite phases coexist on the line d, and no pseudocritical behavior is seen. Two phases coexist along the f lines, and pseudocritical behavior is seen on approaching from $T > 0$. The point b is a triple point but not a pseudotricritical point. Adapted from [34].

Ising spins, which also rules out any pseudocritical behavior in approaching the line from $T > 0$. On the other hand, just as for the case $J > 0$ the f line continues to show two-phase coexistence at $T = 0$ as well as pseudocritical behavior on approaching from $T > 0$. The point b is a triple point but no longer a pseudotricritical point.

Understandably, the zero temperature phase diagram in Figs. 1 and 2 is straightforward, with straight line phase boundaries, because it is influenced only by energy considerations in the absence of any thermal or quantum fluctuation. The region to the right of the f lines in both figures is the one where the D "field" in the Hamiltonian, Eq. (3), is greater than the combined strength of the attractive couplings J and K, so that the energetically preferred state is the one with all spins set to zero.

It will be of interest to see how far the state space geometry encodes the microscopic statistical interactions of the chain. In particular one would like to find out if the state space scalar curvature is representative of the two correlation lengths ξ_1 and ξ_2 and as to how successful it is in encoding the pseudocritical and -tricritical behaviors in the model. In the next section we shall set up two two-dimensional geometries for the BEG model, namely, the ones intrinsic to the D surface and the H surface. Quite satisfyingly, we shall be able to amply demonstrate in our subsequent analysis that the two geometries faithfully represent the underlying correlations in the two order parameters.

III. SECTIONAL THERMODYNAMIC GEOMETRIES OF THE ONE-DIMENSIONAL SPIN-ONE MODEL

In this section we obtain two two-dimensional sectional geometries from the three-dimensional parameter space of the one-dimensional spin-one model and argue why they are a suitable choice for encoding separately the correlations in the spin and the quadrupolar order parameters. Intrinsic thermodynamic metrics on a hypersurface are obtained as a pullback of the ambient metric and physically correspond to restricting spontaneous fluctuations in suitable thermodynamic quantities, the general framework of which was developed in [35] in the context of black hole thermodynamics. In a more direct form the thermodynamic geometry pertaining to restricted fluctuations was used in [36] and [37].[1]

We first set up the equilibrium thermodynamic relations beginning with the free energy per site as the log of the partition function,

$$\psi = \frac{1}{N} \log \sum_{\{S_i\}} \exp[-\beta \, \mathcal{H}_{\text{beg}}]. \qquad (8)$$

It shall be profitable in the following to think of the parameter D as a tunable external field coupled to the quadrupole moment, just as the magnetic field H couples to spin. At the same time the self-interaction parameters J, K are to be thought of as fixed for a given system. The "total" energy per site E and the "internal" energy per site U are obtained as

properly chosen derivatives of the Massieu function

$$-\frac{\partial \psi}{\partial \beta}\bigg|_{H,D} = E = \frac{1}{N} \langle \mathcal{H}_{\text{beg}} \rangle,$$

$$-\frac{\partial \psi}{\partial \beta}\bigg|_{\nu,\mu} = U = \frac{1}{N} \langle \mathcal{H}_{\text{beg}} \rangle + HM - DQ, \qquad (9)$$

where $\nu = \beta H$, $\mu = \beta D$. The differential of the Massieu function can accordingly be expressed either in terms of the variation in total energy or in the internal energy,

$$d\psi(\beta, H, D) = -E \, d\beta + \beta M \, dH - \beta Q \, dD \qquad (10)$$

or

$$d\psi(\beta, \nu, \mu) = -U \, d\beta + M \, d\nu - Q \, d\mu. \qquad (11)$$

If all the fluctuations are unconstrained, then the Riemannian metric of fluctuations is three-dimensional. We take the Massieu function as our starting point and differentiate it twice with respect to the entropic intensive variables β, $\nu = \beta H$, $\mu = \beta D$ to generate the full metric. In our geometric notation we have $x^1 = \beta$, $x^2 = \nu$, $x^3 = \mu$, and for the extensive quantities $X_1 = U$, $X_2 = M$, $X_3 = Q$. Then the three-dimensional thermodynamic metric is the covariance matrix for fluctuations in extensive variables,

$$g_{ij} = \frac{\partial^2 \psi}{\partial x^i \, \partial x^j} = \langle \Delta X_i \, \Delta X_j \rangle. \qquad (12)$$

The inverse of the grand metric in Eq. (12) gives the equilibrium fluctuations in the entropic intensive variables. We write it with raised indices, so we have the following Einstein summation $g^{ik} g_{kj} = \delta^i_j$:

$$(g^{-1})_{ij} \equiv g^{ij} = \langle \Delta x^i \, \Delta x^j \rangle. \qquad (13)$$

From the above metric the fluctuations in the intensive variables T, H, D can be found by obtaining their differential relation with the entropic intensive variables [35]:

$$\Delta T = -\frac{1}{\beta^2} \, \Delta \beta,$$

$$\Delta H = -\frac{\nu}{\beta^2} \, \Delta \beta + \frac{1}{\beta} \, \Delta \nu,$$

$$\Delta D = -\frac{\mu}{\beta^2} \, \Delta \beta + \frac{1}{\beta} \, \Delta \mu. \qquad (14)$$

Using Eq. (13) the fluctuations in intensive variables can be calculated. The variance of T is

$$\langle (\Delta T)^2 \rangle = \frac{1}{\beta^4} \, g^{11}. \qquad (15)$$

The variance of H is

$$\langle (\Delta H)^2 \rangle = \frac{\nu^2}{\beta^4} \, g^{11} - 2 \frac{\nu}{\beta^3} \, g^{12} + \frac{1}{\beta^2} \, g^{22}, \qquad (16)$$

and that of D is

$$\langle (\Delta D)^2 \rangle = \frac{\mu^2}{\beta^4} \, g^{11} - 2 \frac{\mu}{\beta^3} \, g^{13} + \frac{1}{\beta^2} \, g^{33}. \qquad (17)$$

Similarly we could obtain the cross moments such as $\langle \Delta T \, \Delta H \rangle$ etc.

---

[1]For other work on extrinsic curvature in thermodynamic geometry see [38]. Our context and scope are different.

The thermodynamic metric for a system with a given fluctuation constraint can be shown to be the metric induced on the hypersurface generated by the corresponding constraint [35]. Thus, let the coordinates for the parameter space be x^i with $i = 1, \ldots, n$. Then a hypersurface in the parameter space, to which the spontaneous fluctuations are restricted, is given by setting some function f of the coordinates x^i to be zero,

$$f(x^1, x^2, \ldots) = 0. \tag{18}$$

This defines a codimension one hypersurface in the state space, which can be labeled by $n - 1$ coordinates y^a intrinsic to the hypersurface. We shall call it the f surface. The components of the full metric along the f surface give the projection metric in the n-dimensional parameter space,

$$g_{(f)ij} = g_{ij} - \frac{\partial_i f \, \partial_j f}{g^{kl} \partial_k f \, \partial_l f}, \tag{19}$$

where $\partial_i f$ is along the normal to the f surface. In addition to the n-dimensional projection metric we can also write the $(n-1)$-dimensional induced metric on the f surface via the usual pullback of the full metric on the f surface,

$$h_{(f)ab} = g_{(f)ij} \frac{\partial x^i}{\partial y^a} \frac{\partial x^j}{\partial y^b} = g_{ij} \frac{\partial x^i}{\partial y^a} \frac{\partial x^j}{\partial y^b}. \tag{20}$$

The second equality stems from the fact that a tangent vector living on the f surface is orthogonal to the gradient vector $\partial_i f$. The two equivalent metrics in Eqs. (19) and (20) provide complimentary information on fluctuations. Thus the induced metric h_f gives the fluctuations in coordinates intrinsic to the f surface,

$$h_{(f)ab} = \langle (\Delta Y_a \, \Delta Y_b) \rangle_f, \tag{21}$$

and its inverse as

$$h_{(f)}^{ab} = \langle (\Delta y^a \, \Delta y^b) \rangle_f. \tag{22}$$

Here Y_a labels suitable extensive quantities conjugate to the local coordinates defined on the hypersurface. On the other hand, the projection metric directly reads off the f-constrained variance in the quantities defined on the full parameter space,

$$g_{(f)ij} = \langle (\Delta X_i \, \Delta X_j) \rangle_f,$$
$$g_f^{ij} = \langle (\Delta x^i \, \Delta x^j) \rangle_f. \tag{23}$$

For the spin-one model in principle one could restrict the full set fluctuations in as many ways as one could slice the state space. Some of them, however, while mathematically admissible appear to be inaccessible or contrived experimentally. For example, on an M surface wherein the magnetic moment fluctuations are suppressed, the fluctuations in Q would have to peculiarly orchestrated owing to the kinematic coupling between the two. We shall therefore not consider sectional geometries in which the fluctuations in either M or Q are completely suppressed.

We are now ready to construct the two two-dimensional geometries as advertised earlier. Let us first write the geometry obtained by restricting fluctuations in the intensive variable D. A D surface in the β-ν-μ parameter space is the hyperplane

$$f(\beta, \nu, \mu) = \mu - \beta D = 0. \tag{24}$$

A suitable choice of local coordinates on the D surface is

$$y^1 = \beta \quad \text{and} \quad y^2 = \nu, \tag{25}$$

so that global coordinates relate to them on the D surface as

$$\beta(y^1, y^2) = y^1, \quad \nu(y^1, y^2) = y^2, \quad \mu(y^1, y^2) = D y^1. \tag{26}$$

Using Eqs. (24)–(26) in Eq. (20) the components of the induced metric h_D on the D surface are

$$\begin{aligned} h_{(D)11} &= g_{11} + 2D \, g_{13} + D^2 g_{33}, \\ h_{(D)12} &= g_{12} + 2D \, g_{32}, \\ h_{(D)22} &= g_{22}, \end{aligned} \tag{27}$$

where the components g_{ij} have their usual interpretation as variance of extensive quantities; see Eq. (12). Evidently, the results for the induced metric in Eq. (27) can be read off directly by simply setting D to constant in Eq. (11), which gives

$$d\psi = -U_1 \, d\beta + M \, d\nu \quad (D \text{ constant}), \tag{28}$$

where $U_1 = U + QD$ is an enthalpy-like term. By taking second derivatives of ψ with respect to β and ν keeping D constant, we obtain all the components of h_D.

It can checked from Eqs. (23) and (17) that on the D surface the fluctuations in Q are somewhat suppressed in comparison to the unconstrained case while the fluctuations in M remain unaffected:

$$\begin{aligned} \langle (\Delta Q)^2 \rangle_D &= \langle (\Delta Q)^2 \rangle - \frac{1}{\beta^2 \langle (\Delta D)^2 \rangle}, \\ \langle (\Delta M)^2 \rangle_D &= \langle (\Delta M)^2 \rangle. \end{aligned} \tag{29}$$

Not surprisingly, therefore, as we shall see in the next section, the scalar curvature on the Q surface is aligned more with the correlations in the magnetization than in the quadrupolar order.

Similarly, we can develop the geometry of the H surface by projecting out the grand metric along the hypersurface defined by $\nu - \beta H = 0$, where H is a constant. Following the same procedure, the components of the induced metric h_H along the local coordinates $y^1 = \beta$, $y^2 = \mu$ are

$$\begin{aligned} h_{(H)11} &= g_{11} - 2H g_{12} + H^2 g_{22}, \\ h_{(H)12} &= g_{13} - H g_{23}, \\ h_{(H)22} &= g_{33}. \end{aligned} \tag{30}$$

Once again, the components of h_H can be read off by setting H to constant in Eq. (11),

$$d\psi = -U_2 \, d\beta - Q \, d\mu \quad (H \text{ constant}). \tag{31}$$

Here $U_2 = U - MH$ is an enthalpy-like term. One can check from Eqs. (23) and (16) that on the H hypersurface the M fluctuations are weakened while the Q fluctuations remain unrestricted:

$$\begin{aligned} \langle (\Delta M)^2 \rangle_H &= \langle (\Delta M)^2 \rangle - \frac{1}{\beta^2 \langle (\Delta H)^2 \rangle}, \\ \langle (\Delta Q)^2 \rangle_H &= \langle (\Delta Q)^2 \rangle. \end{aligned} \tag{32}$$

Evidently, as our subsequent discussion shall bear out, the scalar curvature on the H surface encodes the correlations in Q instead of M.

We shall term the intrinsic scalar curvatures associated with the H surface and the D surface as the curvatures R_q and R_m respectively. The full three-dimensional grand scalar curvature shall be denoted by R_g, where the subscript g has connotations of the grand canonical ensemble in which all the thermodynamic fluctuations are unrestricted. Finally, we note that the scalar curvatures for all the two-dimensional geometries can be obtained as sectional curvatures along their respective f surfaces of the three-dimensional Riemannian curvature tensor of the grand metric [35,39].

In the following section we obtain the full scaling form of the free energy, including the spin scaling function, using only thermodynamics, and the geometry arising from it.

IV. SINGULAR FREE ENERGY FROM THERMODYNAMICS

For the one-dimensional spin-one model, as for the one-dimensional Ising model [3,5], the scaling form for the free energy (Massieu) near the critical point at $T = 0$ can be written as

$$\psi_s(\beta, h) = n_1 t^a Y\left(n_2 \frac{h}{t^b}\right), \quad (33)$$

where the scaling field are h and $t(\sim e^{-\beta J})$ while $Y(z)$ is the spin scaling function which depends only on the combination $z = ht^{-b}$. Here a and b are the universal scaling exponents, while the constants n_1 and n_2 are nonuniversal and system dependent. As we shall see in the following, the ordering field h equals $H\beta$ near the zero-field critical points and $(H - D + J + K)\beta$ near the wing critical points. Of course, in general the spin-one model has three independent scaling fields [40], so that the spin scaling function would be $Y(h_1/t^b, h_2/t^c)$, with h_1 and h_2 being some linear combination of μ, ν and β. However, mainly for ease of computation, we shall restrict ourselves to the two-dimensional subspace of scaling fields so that Eq. (33) will apply to our spin-one model. In other words we are not taking the most general possible directions of approach to the (pseudo)critical points.

Our investigation of the singular part of the free energy near the pseudocritical and -tricritical points has two related intents. First, given that we are able to obtain the scaling of the free energy on the one hand (Sec. IV A) and the relevant scalar curvature(s) on the other (Sec. V), we could then verify the Ruppeiner equation, Eq. (1), by independent checks on both the sides of the equality. Second, assuming that the Ruppeiner equation is correct, we solve it as a differential equation in the free energy (Sec. IV B), and hence obtain the scaling form(s) of the free energy from among the solutions. In turn it will help validate the Ruppeiner equation if the spin scaling function thus obtained is found to agree with independent numerical checks. As we shall see in the following, the first case is amply verified in the zero-field limit, while the solution of the differential equation in the second case leads to a thermodynamic calculation of the spin scaling function in nonzero field as in [5] where Ruppeiner calculated the same for the one-dimensional Ising model.

Taken together, therefore, we are able to obtain the full scaling form(s) of the free energy from purely thermodynamic considerations as we now proceed to establish.

A. Zero-field scaling of the free energy

On setting the scaling field h to zero in Eq. (33) the scaling function becomes $Y(0) = 1$. This always renders a closed-form expression to the free energy of the one-dimensional spin-one model and, as we show below, it becomes possible to filter out the leading singular terms in the scaling regions.

We first consider the a line of Fig. 1 for which $D < J + K$. We recall that the a line is a locus of pseudocritical points for the magnetization but not for the quadrupolar order. Satisfyingly, it is possible to separate the singular and regular parts of the free energy (or the Massieu function) near the a line, which we shall explain now. Recalling the expression for zero-field Massieu function in Eq. (6) we rewrite it keeping in mind that $D < J + K$ and arrive at an expression of the form

$$\psi = (J + K - D)\beta$$
$$+ \ln\tfrac{1}{2}(1 + e^{(D-J-K)\beta} + e^{-2J\beta} + \sqrt{1 + w}), \quad (34)$$

where

$$w = e^{2(D-J-K)\beta} + 8e^{(D-2J-2K)\beta} + e^{-4J\beta}$$
$$+ 2e^{-2J\beta} - 2e^{(D-3J-K)\beta} - 2e^{(D-J-K)\beta}.$$

The logarithmic term in Eq. (34) goes to zero as $\beta \to \infty$. This is because with $D < J + K$ all the exponential terms within the logarithm, including those comprising w, are less than one and approach zero as β becomes larger. Therefore, we can consider the first term in Eq. (34) as the regular part ψ_r of the free energy near criticality and expect the singular part to be contained in the logarithm. The dominant part of the singular free energy must be that term in the logarithm which is the slowest to decay to zero as β becomes larger. In order to filter out such terms we express the log term for large β as

$$\psi - \psi_r = \ln\left[1 + \tfrac{1}{2}e^{(D-J-K)\beta} + \tfrac{1}{2}e^{-2J\beta} + \tfrac{1}{2}(\sqrt{1 + w} - 1)\right]$$
$$(35)$$

and keep just the linear term in its expansion. However, we must look at all the terms in the expansion of $\sqrt{1 + w}$. This is because it leads to a systematic cancellation of all the terms containing $e^{(D-J-K)\beta}$ or any of its higher powers which are inadvertently generated on expanding the square root term.

The correlation length ξ_1 obtained from Eq. (7) can also be analyzed in a similar manner. In the limit of large β it is seen to go as the inverse of the singular free energy, which is consistent with hyperscaling near the critical point.

The zero-field scaling behavior near the a line with $D < J + K$ is finally obtained as

$$\psi_s = \tfrac{1}{2}\xi_1^{-1} = e^{-2J\beta} \qquad (D < 2K)$$
$$= \tfrac{3}{4}\xi_1^{-1} = 3\,e^{-2J\beta} \qquad (D = 2K)$$
$$= \xi_1^{-1} = 2\,e^{-(2J+2K-D)\beta} \qquad (D > 2K). \quad (36)$$

In the BC limit $K = 0$ it is easily seen that we get different scaling behaviours for $D < 0$, $D = 0$, and $D > 0$.

We now consider on the zero-field line the point $D = J + K$, which is a triple as well as a pseudotricritical point. As can be checked from its expression in Eq. (34) the free energy now goes to zero in the zero temperature limit. Its expression simplifies to

$$\psi = \ln\left(1 + \tfrac{1}{2}e^{-2J\beta} + \tfrac{1}{2}e^{-2J\beta}\sqrt{1 + 8e^{(3J-K)\beta}}\right). \quad (37)$$

After a simple expansion of the logarithm we take the dominant part of the free energy as the one which is the slowest to decay as the pseudotricritical point is approached from nonzero temperatures. Depending on whether K is less than, equal to, or greater than $3J$ we have three cases for the zero-field scaling near the pseudotricritical point with $D = J + K$:

$$\begin{aligned}
\psi_s &= \sqrt{2}\, e^{-(J+K)\beta/2} \quad &(K < 3J) \\
&= 2\, e^{-2J\beta} \quad &(K = 3J) \\
&= e^{-2J\beta} \quad &(K > 3J).
\end{aligned} \quad (38)$$

At the pseudotricritical point both correlation functions ξ_1 and ξ_2 diverge with the following asymptotic relation to the singular free energy:

$$\begin{aligned}
\xi_1 &= 2\,\xi_2 = \psi_s^{-1} \quad &(K < 3J) \\
&= \xi_2 = \tfrac{2}{3}\psi_s^{-1} \quad &(K = 3J) \\
&= 2\,\xi_2 = \psi_s^{-1} \quad &(K > 3J).
\end{aligned} \quad (39)$$

Finally, we consider the f line on which $D = |H| + J + K$. With nonzero H it is easier to work with the numerical solutions for the eigenvalues of the transfer matrix. The f line is a pseudocritical point for both the magnetic order and the quadrupolar order when approached from nonzero temperatures. For nonzero field both order parameters have the same correlation length ξ_1 [34]. Just as for the pseudotricritical point the free energy goes to zero on the f line, and its singular part is double the inverse correlation length

$$\psi_s = \tfrac{1}{2}\,\xi_1^{-1} = e^{-(J+K)\beta/2} \quad (D = |H| + J + K). \quad (40)$$

B. Spin scaling function $Y(z)$ from geometry

Having obtained the zero-field scaling of the free energy we now turn to the calculation of the spin scaling function $Y(z)$ using thermodynamic geometry. Our derivation of the spin scaling function closely follows Ruppeiner's calculation for the same in [5].

We first express the two-dimensional scalar curvature R as a ratio of determinants involving derivatives of the free energy [4,5]:

$$R = -\frac{1}{2}\frac{\begin{vmatrix} \psi_{,11} & \psi_{,12} & \psi_{,22} \\ \psi_{,111} & \psi_{,112} & \psi_{,122} \\ \psi_{,112} & \psi_{,122} & \psi_{,222} \end{vmatrix}}{\begin{vmatrix} \psi_{,11} & \psi_{,12} \\ \psi_{,21} & \psi_{,22} \end{vmatrix}^2}. \quad (41)$$

It can be checked that near the (pseudo)critical point, under sufficiently general circumstances, the background free energy contribution to R is insignificant in comparison to the singular term so that in the equation for R above we can replace ψ by ψ_s everywhere. With this understanding the Ruppeiner equation becomes a third-order PDE for ψ_s. One can further check that on substituting the scaling form of the free energy from Eq. (33) in Eq. (41), and hence in the Ruppeiner equation (1), all factors of the powers of $t(\beta)$ and h cancel out, resulting in a third-order ordinary differential equation (ODE) for $Y(z)$ [4,5]. This is very much in keeping with the conjectured exactness of the Ruppeiner equation near criticality so that the only unknowns are the *universal* exponents and the *universal* scaling function. Putting $b = ma$ in Eq. (33), with m being any positive constant, and temporarily rescaling z to $z = n_2 h/t^b$ the Ruppeiner equation is obtained in terms of the derivatives of Y, the constant m, and the free variable z as

$$\begin{aligned}
2\kappa&(m^2 z Y'Y'' + (m-1)^2 Y'^2 - Y Y'')^2 \\
&= -mY\big\{(m-1)Y'^2\big[(m-2)nY^{(3)}z + (m-1)^2 Y''\big] \\
&\quad + Y'\big[m^3 Y^{(3)} z^2 Y'' + (m-1)YY^{(3)} + (3m-1)mzY''^2\big] \\
&\quad - Y''\big[m^3 z^2 Y''^2 + mYY^{(3)}z + 2(2m-1)YY''\big]\big\},
\end{aligned} \quad (42)$$

where $Y', Y'', Y^{(3)}$ denote the first, second, and third derivatives of Y with respect to z.

In order to solve for $Y(z)$ we assume it to be an even function of z and expand it as an even series in z with unknown coefficients,

$$Y(z) = a_0 + a_2 z^2 + a_4 z^4 + \cdots. \quad (43)$$

Clearly, about the zero-field line of Fig. 1 $Y(z)$ will be an even function of z although it is not *a priori* clear whether the scaling function is symmetric about the f line. As our numerical studies seem to suggest, probably there are different scaling functions $Y_\pm(z)$ above and below the f line. In any case we shall restrict our investigation to regions above the f wings and continue to assume an even symmetry for the scaling function $Y_+(z)$ there. Our numerical checks do confirm this form for $Y_+(z)$ even as we are unable to find a satisfactory explanation for the same.

Furthermore, the usual assumption $Y(0) = 1$ sets the coefficient $a_0 = 1$. Therefore, of the three constants of integration generated by integrating the third-order ODE in Y only one is left undetermined. Plugging in the series expansion of $Y(z)$ from Eq. (43) into Eq. (42) one obtains

$$\begin{aligned}
0 =\ & (m(2m-1) - \kappa) \\
& + \frac{m\big(16a_2^2 m^3 - 24a_2^2 m^2 + 14a_2^2 m - 3a_2^2 + 6a_4\big)}{a_2} z^2 \\
& + O(z^4).
\end{aligned} \quad (44)$$

Further simplification results from an additional input coming from thermodynamic geometry. As we shall be establishing in the next subsection, for the one-dimensional spin-one model the relevant section curvatures are exactly inverse those of the free energy, namely, $\kappa = 1$ in the pseudocritical and the pseudotricritical limit. Barring a few, most of the checks are numerical. On approaching the a line the

curvature R_m follows the Ruppeiner equation (1) with $\kappa = 1$ while R_q remains finite, and on approaching the f line and the pseudotricritical point c both R_m and R_q follow the Ruppeiner equation with $\kappa = 1$. See Fig. 7(c) below for an example.

This sets the value of the positive constant m to unity as can easily be checked by putting $\kappa = 1$ in

$$m = \tfrac{1}{4}(\sqrt{8\kappa + 1} + 1),$$

which is obtained by setting to zero the coefficient of the zeroth power of z in Eq. (44). Therefore, geometry quickly leads to the result that for the one-dimensional spin-one model the exponents $a = b$.

Finally, Eq. (44) simplifies to

$$0 = \frac{3\left(a_2^2 + 2a_4\right)}{a_2} z^2 + \frac{\left(5a_2^4 + 22a_4 a_2^2 + 30a_6 a_2 - 36a_4^2\right)}{a_2^2} z^4$$
$$+ O(z^6). \tag{45}$$

Setting the coefficient of each power of z to zero leads to a series solution for Y which has the closed-form expression,

$$Y(z) = \sqrt{1 + (z/n)^2}, \tag{46}$$

where we have reverted to $z = h/t^a$ as in in Eq. (33) and the constant n is related to a_2 and n_2.

Combining with the results of the previous section we can now present the formal structure of the singular free energy for the one-dimensional spin-one model,

$$\psi_s(t, h) = n\, t\, Y\left(\frac{h}{n\,t}\right)$$
$$= \sqrt{(n\,t)^2 + h^2}. \tag{47}$$

This is the key result of this section. The different values of the constant factor n are the ones multiplying the exponentials in the zero-field scaling expressions for ψ_s obtained in the previous Sec. IV A. Thus, Eq. (36) for the scaling near the a line has $n = 1, 3, 2$, Eq. (38) near the pseudotricritical point has $n = \sqrt{2}, 2, 1$ and Eq. (40) near the f line has $n = 1$. The reduced temperature t is always defined here such that the exponents $a = b = 1$. The reduced temperature for the spin-one model is not always equal to $e^{-\beta J}$ as in the one-dimensional Ising case but, as we saw in the previous subsection, is of the more general form $e^{-\beta X}$ where X is a linear combination of the coupling strengths in the Hamiltonian, with its form depending on the relative strength of the coupling terms. Finally, as mentioned earlier, the ordering field is $h = \beta H$ in the vicinity of the pseudocritical a line and the pseudotricritical point, while around the upper and lower f lines it is $h = (H - D + J + K)\beta$ and $h = (H + D - J - K)\beta$ respectively.

As alluded to earlier, numerical checks show that the differential equation (42) for $Y(z)$ with $\kappa = 1$ is not satisfied inside the f wings. This suggests that the form of the scaling function $Y_-(z)$ must be different. We defer a detailed investigation of this observation to the future.

Having utilized the strong conjecture of Ruppeiner to obtain the scaling function from thermodynamic geometry we turn our attention now to the investigation of the thermodynamic curvature vis-à-vis the correlation length, a relation

which encompasses both the strong and the weak aspects of the conjecture. We shall examine the curvatures R_q and R_m for different parameter ranges and also comment on the three-dimensional scalar curvature R_g.

V. GEOMETRY OF THE $J > 0$ CASE, THE ONE-DIMENSIONAL BEG AND BC MODELS

We now discuss the thermodynamic geometry of the one-dimensional BEG model, namely, the spin-one model with $J > 0$. The Griffiths model ($J = 0$) shall be discussed separately in the next section. The zero temperature phase diagram for this case is given in Fig. 1. As discussed earlier, on line a the correlation lengths of the two order parameters M and Q are different, $\xi_1 \neq \xi_2$, while at the pseudotricritical point c and on the f line $\xi_1 = \xi_2$.

From several scalar curvature vs correlation length plots we shall see that ξ_1 and ξ_2 correspond well with the scalar curvatures R_m and R_q, respectively, for a wide range of parameter values, far beyond criticality. There are apparent variations to the theme, however, possibly reflecting attributes of R apart from its association with the magnitude of the correlation length. We hope to address these observations in a future investigation.

As a warm-up and to set the stage for what follows, we do a lightning review of the geometry of the one-dimensional ferromagnetic Ising model first discussed in [19,20]. The free energy and the correlation function can be obtained via the transfer matrix in the standard manner. The singular part of free energy near the pseudocritical point $T = 0, H = 0$ in the β-H plane has the well-known scaling form [3]

$$\psi_s = e^{-2J\beta}\left[1 + \left(\frac{H\beta}{e^{-2J\beta}}\right)^2\right]^{1/2}, \tag{48}$$

and the correlation length is obtained as

$$\xi^{-1} = \log\left(\frac{e^{2\beta H} + W + 1}{e^{2\beta H} - W + 1}\right), \tag{49}$$

where $W^2 = -2e^{2\beta H} + e^{4\beta H} + 4e^{2(H+2J)\beta} + 1$, while the scalar curvature is obtained as a simple expression [20]

$$R = -\cosh(\beta H)\frac{1}{\sqrt{\exp(-4J\beta) + \sinh^2(\beta H)}} - 1. \tag{50}$$

It can be checked that R follows the Ruppeiner equation at the pseudocritical point ($H = 0, \beta \to \infty$) with the proportionality $\kappa = 1$ and $-R \to 2\xi$. Satisfyingly, even for nonzero magnetic field, which takes the system away from criticality, the curvature R closely "envelops" the correlation length with the former asymptoting to -2 as ξ decays to zero for large β. Trends in R are shown in Fig. 3(a) for zero field and Fig. 3(b) for nonzero field.

Thus, an exploration of the one-dimensional Ising model reinforces both the strong and the weak ends of Ruppeiner's conjecture. Both features will appear as a common theme in the geometry of the one-dimensional spin-one model to be discussed below. In particular, the weak end of Ruppeiner's conjecture, which has not been sufficiently emphasized in the literature, occurs as a recurring motif in this work.
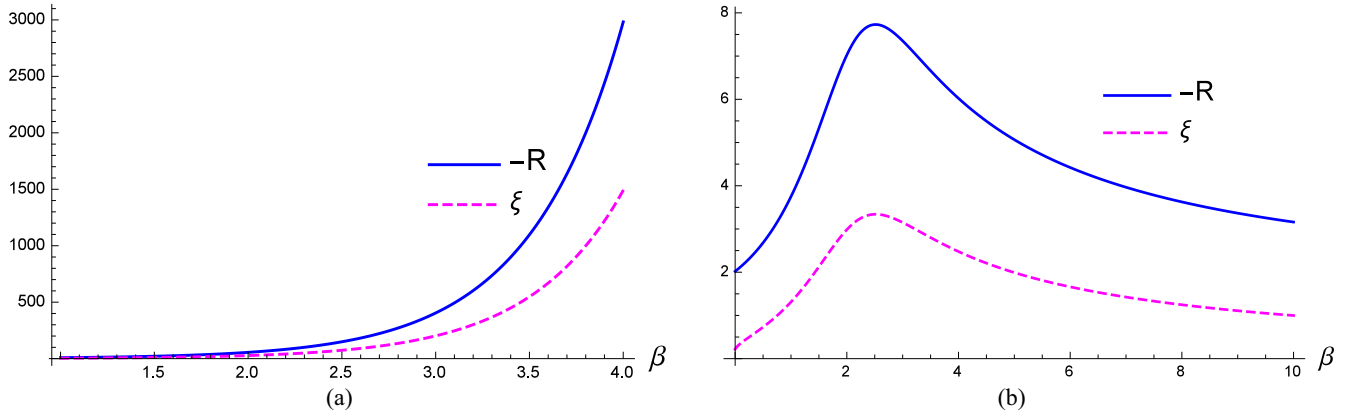
FIG. 3. Temperature plots of $-R$ and ξ for the one-dimensional Ising model with the coupling J set to unity. (a) The magnetic field is set to zero. Curvature goes as twice the correlation length at low temperatures. (b) The magnetic field is nonzero and is set to $H = 0.1$. Curvature maintains a steady distance with the correlation length.

In the following subsections we shall sort our observations of the scalar curvatures R_q, R_m, and R_g for different relative strengths of the couplings $H, D, J,$ and K.

A. The zero-field case

The region of interest in this subsection will be the pseudocritical a line and the pseudotricritical c point of Fig. 1, and we shall observe the curvature, correlation length, or the free energy as we approach these points from nonzero temperatures. We shall discuss the cases $J > K$ and $J = K$ separately, and in both we shall deal first with R_q followed by R_m and R_g, scanning in each case D values to the left of, at, and beyond the pseudotricritical point.

1. The case J > K

This case is the most relevant to the BEG model inasmuch as it refers to $He^3 - He^4$ mixtures since for such mixtures K is much less than J. Similarly, it is also relevant to the BC model for which $K = 0$. The a line, the pseudotricritical point c, and the part of x axis to its right in Fig. 1 constitute the zero-field line. The a line is a pseudocritical line with respect to M fluctuations but not for Q fluctuations.

First, we consider R_q and ξ_2 on the whole of the zero-field line. We note that we can obtain a closed-form expression for R_q by setting H to zero in the thermodynamic metric defined

on the constant H surface, Eq. (31). While the zero-field expression for R_q is too large to be shown here, we obtain much smaller expressions for some special cases which we shall present on appropriate occasions. It is seen that for values of $D < K - J$ the magnitude of R_q maintains an approximately constant distance with the correlation length ξ_2, with R_q converging to -1 and the latter to zero as T tends to zero.

At $D = K - J$ the curvature R_q converges to a value slightly less than -1, which depends only on the ratio K/J, with the minimum value of -1.25 in the BC limit $K = 0$ irrespective of the value of J. In Figs. 4(a) and 4(b) where we plot together the variation in the magnitude of R_q and ξ_2 with respect to β, it can be seen that they maintain a separation of approximately one lattice unit for $D \leqslant K - J$. We also note that the association of the scalar curvature to the correlation length has no connection to criticality here.

For $K - J < D < K + J$ the curvature R_q does not match ξ_2 for the full range of temperature. While it parallels with ξ_2 for small values of β (high temperature) it soon enough diverges away to more and more negative values, Fig. 4(c). The negative divergence, however, is always less than or equal to the rate of divergence of ξ_1 or, equivalently, the negative divergence of R_m as discussed below. While the apparently anomalous divergence could possibly provide some clue to the nature of underlying statistical interactions, we shall defer such questions to a future investigation.
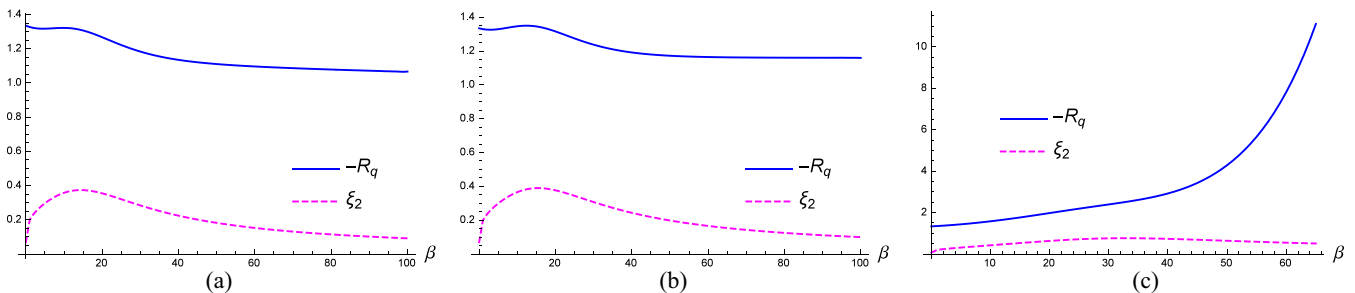

FIG. 4. Plots of $-R_q$ and ξ_2 against β for different ranges of D values, with $H = 0, D < J + K,$ and $K < J$. In all subfigures $J = 0.05, K = 0.03$. (a) $D = -0.029 < K - J$, (b) $D = -0.02 = K - J$, and (c) $D = 0.05 > K - J$. In (a) and (b) the curvature remains almost parallel to the decaying correlation length, while in (c) it diverges away after running parallel for a while.
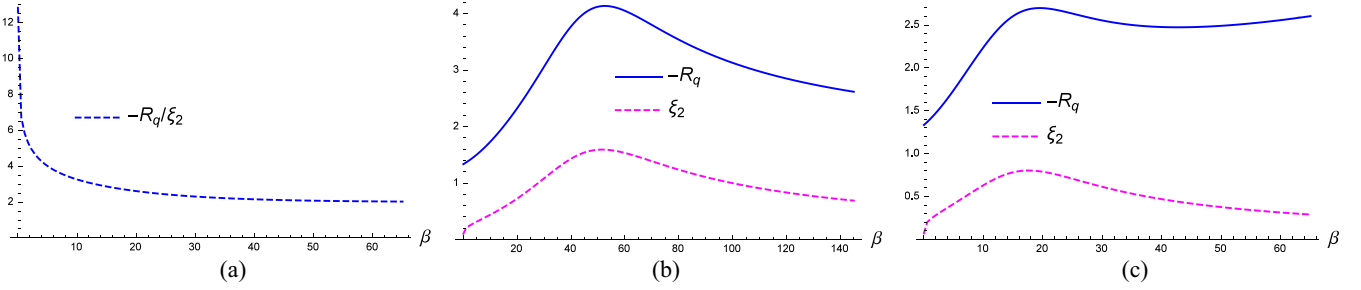
FIG. 5. Plots of $-R_q$ and ξ_2 against β for different ranges of D values, with $H = 0$, $D \geqslant J + K$, and $K < J$. In all subfigures $J = 0.05$, $K = 0.03$. In (a) with $D = 0.08 = K + J$(pseudotricritical point), the ratio $-R_q/\xi_2$ is plotted against the inverse temperature. In (b) with $D = 0.09 < 2J$ and in (c) with $D = 0.11 > 2J$ both R_q and ξ_2 are plotted against β.

At the pseudotricritical point $D = J + K$, the negative of R_q and ξ_2 both remain parallel and diverge asymptotically as $e^{(J+K)\beta/2}$, which is in line with Eq. (38). It can be checked that asymptotically $-R_q \sim 2\,\xi_2$, which is consistent with Eq. (39) with $R_q \to \psi^{-1}$ in the pseudotricritical limit. Significantly, even at temperatures much farther from zero R_q is already approximately twice ξ_2 as can be seen in Fig. 5(a).

Beyond the tricritical point, for $J + K < D < 2J$, the magnitude of R_q and that of ξ_2 again run parallel to each other with the former converging to -2 and the latter decaying to zero as T tends to zero. This is shown in Fig. 5(b). For $D = 2J$ the curvature R_q converges to a value between -2 and -4 with the latter value fixed for the BC limit irrespective of J. For $D > 2J$ R_q behaves anomalously and diverges to negative infinity as shown in Fig. 5(c).

In the BC limit ($K = 0$) the tricritical point expression for R_q simplifies to

$$R_q = \frac{\mathcal{N}_1}{\mathcal{D}_1} \quad (D = J, H = 0, K = 0), \tag{51}$$

where $\mathcal{N}_1$ and $\mathcal{D}_1$ are given in Eq. (A1) in the Appendix.

We now consider R_m and the three-dimensional scalar curvature R_g on the zero-field line. Closed-form expressions are not available for these curvatures since the eigenvalues of the transfer matrix with nonzero H are to be obtained by solving a cubic equation. The curvature R_m and the correlation length ξ_1 run parallel to each other up to the pseudotricritical point, i.e., for $D \leqslant J + K$. The ratio of the curvature to correlation length is fully consistent with Eq. (36) for all range of values of the parameter D, with $R_m \to \psi_s^{-1}$ towards zero temperature. In Fig. 6(a) we observe that the ratio R_m/ξ_1 soon enough ap-

proaches a value of 2, which, for the chosen parameter values in the figure, is consistent with Eq. (36). The full curvature R_g is seen to closely parallel the curvature R_m. In Figs. 6(b) and 6(c) we plot together the products of R_m and R_g with ψ_s for different values of D, with the latter subfigure at the pseudotricritical value $D = J + K$.

We note here that the two-dimensional scalar curvature R_m is seen to follow the Ruppeiner equation near criticality with the proportionality $\kappa = 1$. While R_g still follows the Ruppeiner conjecture at criticality in that it goes as the inverse of singular free energy, the proportionality constant κ does not appear to be a universal number, though it is still of order one. There are patterns to the variation. For example, at the pseudotricritical point for $K < 3J$ the constant $\kappa = 3.5$, while for $K \geqslant 3J$ it is equal to 3. A fuller understanding of this issue will necessary involve the full scaling form of the free energy with three scaling fields t, h_1, and h_2 and exponents a, b, and c [40], a line we do not pursue here. For work relating the three-dimensional scalar curvature to the singular free energy in systems at finite T_c we refer the reader to [17].

Beyond the pseudotricritical point while the correlation length ξ_1 decays to zero at low temperatures R_m does not match with ξ_1 and diverges in the negative direction.

2. The case $J = K$

For the case when the spin coupling strength is equal to the quadrupole coupling, the curvature R_q shows an excellent correspondence with ξ_2 for all values of D. For $D < J + K$ the curvature R_q runs parallel to ξ_2 and asymptotes to -1 as the correlation length tends to zero for low temperatures. Simi-
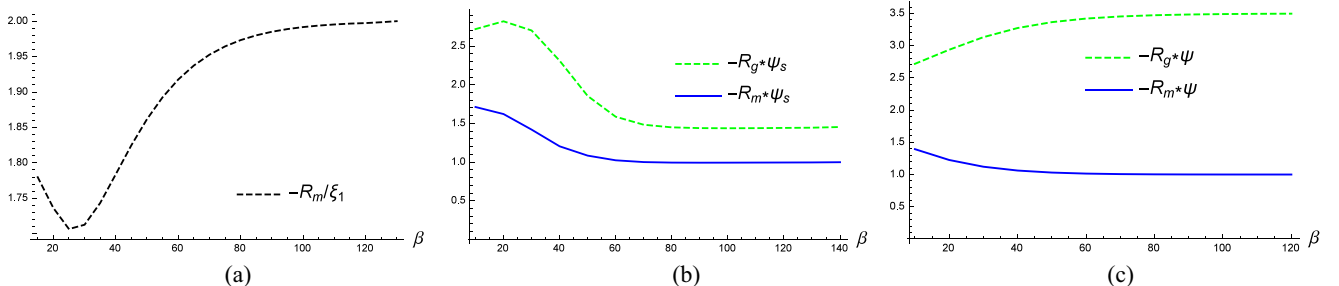

FIG. 6. In all subfigures $J = 0.05$, $K = 0.04$. (a) Plot of R_m/ξ_1 vs β with $D = 0.02$. (b) Plots of $-R_g \times (\psi - \psi_r)$ and $-R_m \times (\psi - \psi_r)$ vs β for $D = 0.082$. (c) Similar as (b) but with $D = J + K = 0.09$.
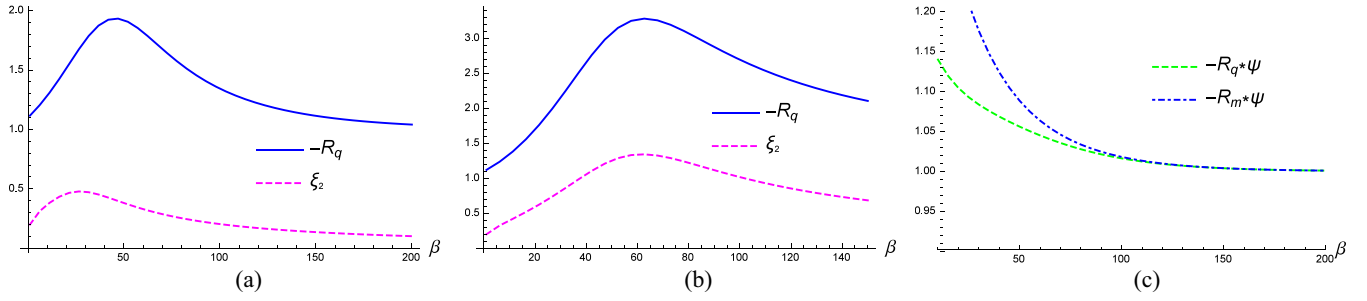
FIG. 7. In all subfigures $J = K = 0.03$ and $H = 0$. (a), (b) Plots of R_q and ξ_2 vs β for $D = 0.05$ and $D = 0.07$, respectively. (c) Plots of $-R_q\,\psi$ and $-R_m\,\psi$ are shown at the pseudotrictritical point for $D = J + K = 0.06$.

larly, for $D > J + K$ it asymptotes to $-3/2$ as ξ_2 tends to zero. For the pseudotricritical point $D = 2J$, $-R_q$ and ξ_2 diverge to infinity as $e^{J\beta}$ with $R_q \to 2\,\xi_2$ at low temperatures, consistent with Eqs. (38) and (39). For $J = K$ the zero-field expression for R_q reduces considerably, and it can be expressed as the fraction

$$R_q = \frac{\mathcal{N}_2}{\mathcal{D}_2}, \qquad (52)$$

where the numerator and denominator are given in the Appendix, Eq. (A2). In Fig. 7(a) the curvature R_q and ξ_2 are plotted for a value of $D < J + K$ and in Fig. 7(b) for $D > J + K$. For both cases there is a very good correspondence between curvature and correlation length as discussed above.

R_m corresponds well with ξ_1 up to the pseudotricritical point. For $D < 2J$ the curvature R_m equals twice ξ_1 for low temperatures, while for the pseudotricritical point $D = 2J$ it equals ξ_1 at low temperatures in line with Eq. (39). For $D < 2J$ the asymptotic divergence of ξ_1 and R_m is $e^{2J\beta}$, while at the pseudotricritical point it is $e^{J\beta}$, all of which follow Eq. (38). Once again, beyond the pseudotricritical point R_m does not match with ξ_1 and diverges in the negative direction in a manner similar to the $J > K$ case.

In Fig. 7(c) the product of the magnitude of R_m and R_q with the free energy is plotted for the pseudotricritical value of D. The two curvatures are seen to approach each other, and the product quickly reaches a value of $\kappa = 1$ following the Ruppeiner equation. Furthermore, for the three-dimensional curvature the product $R_g\psi$ approaches 3.5 as mentioned earlier (not shown in the figure).

3. The case $J < K$

For this parameter range we focus mainly on the pseudotricritical point at $D = J_K$ where the curvature R_q has a more nuanced detailed scaling behavior compared to the previous two cases $J > K$ and $J = K$. Here we shall also be tracking the values of the quadrupole moment and its fluctuation $\langle(\Delta Q)^2\rangle$, the reason for which will soon become clear.

For $J < K \leqslant 3J$ R_q diverges to negative infinity as $e^{(J+K)\beta/2}$, and follows the Ruppeiner equation with $\kappa = 1$. For $K < 3J$ the quadrupole moment approaches $1/2$ at zero temperature, and its fluctuation diverges as $e^{(J+K)\beta/2}$. At $K = 3J$ the quadrupole moment approaches $2/3$ at zero temperature. For $3J < K < 5J$ the curvature continues to diverge to minus infinity at the same rate as the correlation length ξ_2, which now diverges as $e^{2J\beta}$. However, now at low temperatures the product $-R_q\psi_s = \kappa$ is less than 1, and it decreases substantially as K approaches $5J$. For example, as K increases from 0.149 to 0.1499, for $J = 0.03$, κ decreases almost ten times from $\frac{299}{14\,400}$ to $\frac{2999}{1\,440\,000}$. Thus, while R_q still diverges to negative infinity in this parameter range, it does not strictly follow the Ruppeiner equation. This can be seen in Fig. 8(a), where R_m clearly follows the Ruppeiner equation but not R_q. Meanwhile, for all values of $K > 3J$ the quadrupole moment tends to 1 and its fluctuation goes as $e^{(5J-K)\beta}$. Therefore, as K approaches $5J$ the divergence in quadrupole fluctuations keeps flattening. This might appear curious since the quadrupole-quadrupole correlation length ξ_2 grows steadily as $e^{2J\beta}$.

At $K = 5J$, the quadrupole fluctuation completely flattens and approaches a fixed value of 4. Exactly paralleling this situation, the curvature R_q also stops diverging and asymptotes
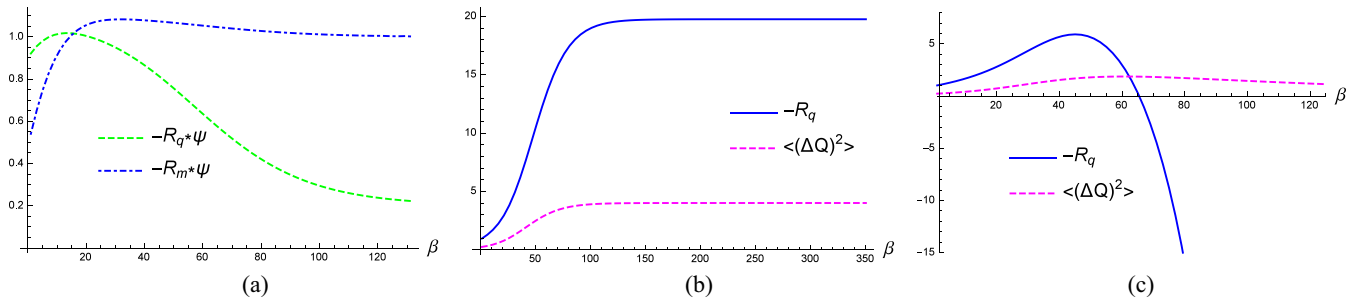

FIG. 8. Zero-field plots with D at pseudocritical values $D = J + K$ and $K > J$. (a) Plot of the products of the singular free energy ψ with R_q and R_m, for $J = 0.03$, $K = 0.14 < 5J$, $D = 0.17$. (b) Plot of R_q and $\langle(\Delta Q)^2\rangle$ vs β with (b) $J = 0.03$, $K = 0.15 = 5J$, $D = 0.18$ and (c) $J = 0.03$, $K = 0.16 > 5J$, $D = 0.19$.

to a fixed negative value of $-79/4$ at $K = 5J$, as seen in Fig. 8(b). The correlation length continues to diverge at the same rate as before. For $K > 5J$ the quadrupole fluctuation decays to zero in the zero temperature limit. Now the curvature R_q diverges to *positive* infinity at the same rate as the correlation length, namely, as $e^{2J\beta}$. This is shown in Fig. 8(c). This is interesting because in general the scalar curvature diverges to negative infinity at the critical point. For $D > J + K$ the curvature R_q diverges to positive infinity as $e^{(D-2J)\beta}$ after briefly following the correlation length.

The apparent discrepancy between the divergence of the quadrupole correlation length and at the same time the decay of the quadrupole fluctuations at the pseudotricritical point is mathematically understood by examining the expression for the quadrupole fluctuation [34],

$$\frac{\partial^2 \psi}{\partial \mu^2} = \frac{1}{N}\left\langle \left(\sum_{i=1}^{N} \Delta Q_i\right)^2 \right\rangle = \frac{Q(1-Q)}{1 - \lambda_3/\lambda_1}, \quad (53)$$

so that while at the pseudotricritical point $\lambda_3 \to \lambda_1$ which implies $\xi_2 \to \infty$, the numerator could compete with the zero in the denominator if $Q \to 1$. This is more pronounced for $K > 5J$ when the quadrupole fluctuation now decays to zero while the correlation length continues to diverge as before. It is significant that the curvature R_q tracks this peculiar trend in quadrupole correlations.

The curvature R_m follows the Ruppeiner equation for all $K > J$ and for all $D \leqslant K + J$. The asymptotic ratio between R_m and the singular free energy (and with ξ_1) is reached much before pseudocriticality thus again emphasizing the weak conjecture of Ruppeiner. Beyond the pseudotricritical point R_m behaves exactly as in the previous cases in that it anomalously diverges to negative infinity at zero temperature even as ξ_1 decays to zero.

B. The case $H \neq 0$: The f line and beyond

The non-zero-field region in Fig. 1 comprises the f line, the regions to its left and right, and the neighborhood of the pseudotricritical point. We note that since we cannot obtain closed-form expressions for non-zero-field scalar curvatures, all the checks will be numerical.

On the f line both curvatures R_q and R_m diverge and follow the Ruppeiner equation with $\kappa = 1$ as shown in Fig. 9. As is apparent from the figure, both curvatures merge into each other at low temperatures, which is consistent with the fact there is only one correlation length ξ_1 for nonzero field. The scaling of scalar curvatures is $e^{(J+K)\beta/2}$, which follows from Eq. (40). The three-dimensional curvature R_g more or less follows the curvature R_m so we do not describe it separately here. In order to explore further the geometry of nonzero H we refer to Fig. 11, which records trends in R_m and R_q in nonzero field. The values of parameters J and K are fixed at 0.1 and 0.09, respectively, in the figure. Turning our attention first to the vicinity of the red f line we notice that starting from small nonzero values of H onwards there is a wedge-shaped band around the f line, bordered by blue dots on the left and green squares on the right. Within this "f band" it is observed that the two curvatures R_m and R_q overlap very strongly at low
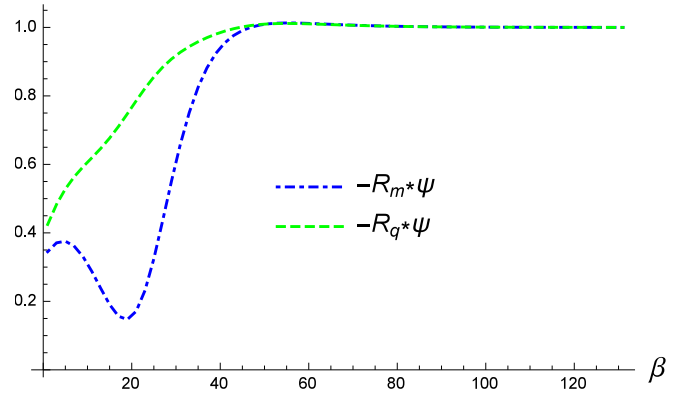

FIG. 9. Plot of the products $R_m\psi$ and $R_q\psi$ vs β on the f line. The parameters $J = 0.03$, $K = 0.1$, $H = 0.01$, $D = H + J + K = 0.14$.

temperatures and show an excellent correspondence with the decaying correlation length.

Further, the band is characterized by an additional high-temperature local maximum (or a "hump") in both the R_m vs β and R_q vs β plots; see Fig. 10. While the hump appears as a prominent feature in the geometry there appears to be no such indication in the plot of the correlation length in Fig. 10. Given the connection between the scalar curvatures and the underlying microscopic interactions it would be interesting to see if there really is any hidden microscopic physics that such a feature seems to be shining a light on. A possible clue to the analytical origins of the hump feature is that the numerically obtained boundaries of the f band are always straight lines as can be seen in the figure. We observe that at smaller values of H (about 0.05 in the figure), the f band shrinks to zero so that the "hump" feature is altogether absent close enough to the pseudotricritical point. Therefore, geometry seems to suggest that the neighbourhood of the pseudotricritical point is qualitatively different, and establishing the correctness, or otherwise, of this geometric description could be an interesting future investigation. While the overlap is excellent within the f band the two curvatures begin to separate on moving leftwards but still maintain a somewhat constant separation till the boundary marked by green "tilde"-shaped symbols is
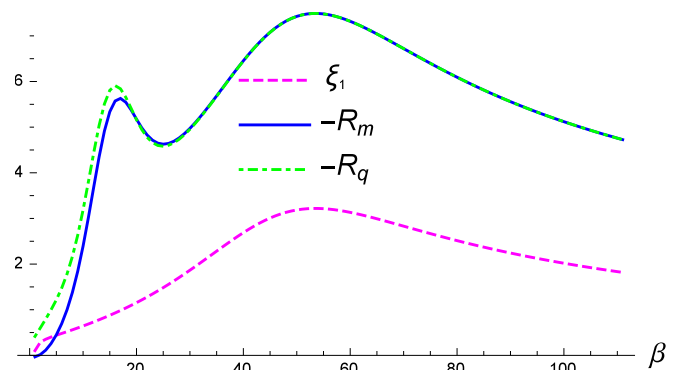

FIG. 10. Representative plot of R_m, R_q, and ξ_1 in the f band, with parameter values $J = 0.1$, $K = 0.09$, $D = 0.45$, and $H = 0.25$. The hump in the curvatures and their substantial overlap is noticeable.
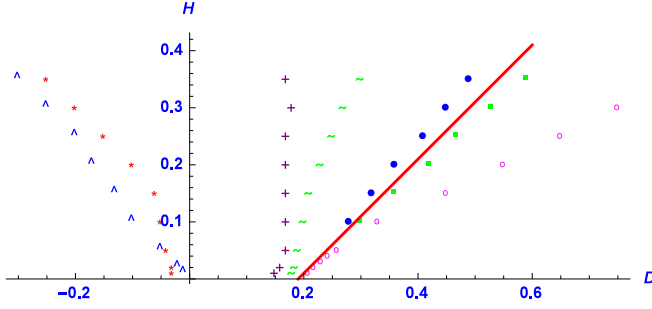
FIG. 11. Diagram showing trends in the curvatures R_m and R_q in the H-D plane with $J = 0.1$, $K = 0.09$.

reached; see Fig. 11. R_q diverges to negative infinity from this point leftwards up to the boundary marked by the blue "caret" symbols, beyond which it diverges towards positive infinity. Similarly, moving leftwards from f band the curvature R_m shows a positive divergence in the region bordered by the purple "plus" symbols and red "asterisk" symbols, beyond which it shows a negative divergence. Moving to the right of the f band, it is seen that R_m, R_q and the correlation length have a good match till the boundary marked by pink "open circles," beyond which both curvatures diverge to negative infinity. We recall that everywhere in the non-zero-field region except on the f line the correlation length always decays to zero. The three-dimensional curvature R_g more or less follows the curvature R_m, so we do not describe it separately here.

Admittedly, we do not understand the physics behind the several sign changes of the curvatures here, but given that the sign of the scalar curvature is commonly associated with the nature of underlying statistical interactions, it is important to record patterns in its variation. We hope to return to this issue in the future.

VI. $J = 0$ CASE, THE ONE-DIMENSIONAL GRIFFITHS MODEL

We now obtain the free energy scaling and the scalar curvatures for the Griffiths model, namely, the $J = 0$ limit of the BEG model. The zero temperature phase diagram for the one-dimensional Griffiths model was described earlier in Sec. II and represented in Fig. 2. The absence of the spin coupling strength changes the phase structure of the general BEG model qualitatively so that now the whole of the x axis is noncritical and the point at $D = K$ in zero field is no longer (pseudo)tricritical but just a triple point. The f line ($D = H + K$) continues to remain (pseudo)critical, but here too, as we show, for $H < K/4$ the rate of correlation length divergence decays to zero as H tends to zero at the triple point.

A. Scaling behavior near the pseudocritical line

The absence of the spin coupling strength J simplifies the transfer matrix in Eq. (5) enough to render closed-form expressions for two eigenvalues, with the third eigenvalue identically zero:

$$\lambda_{\pm} = \tfrac{1}{2} e^{-(D+H)\beta} \left(e^{(D+H)\beta} + e^{(2H+K)\beta} + e^{\beta K} \pm \sqrt{W} \right), \quad (54)$$

where

$$W = \left(e^{(D+H)\beta} + e^{(2H+K)\beta} + e^{K\beta} \right)^2 + 4 \left(e^{(D+H)\beta} + e^{(D+3H)\beta} - e^{(D+H+K)\beta} - e^{(D+3H+K)\beta} \right).$$

From the above equation we can calculate the free energy ψ as log (λ_+) and the correlation length ξ as $1/\log(\lambda_+/\lambda_-)$. Starting with the free energy closed-form expressions can be obtained for R_m, R_q, and R_g. We note that while the numerical values of the curvatures in this section can be obtained from those of the previous section on setting $J = 0$, closed-form expressions were not available earlier for nonzero H. All the same, the closed-form expressions are too large to be presented here.

We can obtain the scaling form for the free energy on the f line by obtaining its approximate expression for large values of β:

$$\psi \underset{\beta \to \infty}{\to} \tfrac{1}{2} e^{-2H\beta} + \tfrac{1}{2} \sqrt{4 e^{2\beta H} + 4 e^{4\beta H} + e^{\beta K}}. \quad (55)$$

The leading singular term of the free energy and its relation to the correlation length on the f line with $D = H + K$ can now be obtained as

$$\psi_s = \xi^{-1} = e^{-2H\beta} \qquad (H < K/4)$$

$$= \frac{1 + \sqrt{5}}{2\sqrt{5}} \xi^{-1} = \frac{1 + \sqrt{5}}{2} e^{-K\beta/2} \quad (H = K/4)$$

$$= \frac{1}{2} \xi^{-1} = 2 e^{-K\beta/2} \qquad (H > K/4). \quad (56)$$

We already see a noticeable difference in the scaling behavior on the f line of the Griffiths model, Eq. (56), as compared to that in the BEG model, Eq. (40), in that for $H < K/4$ the singular free energy in the Griffiths model weakens until it disappears at the triple point at $H = 0$. In fact, this is the only instance in the report where the scaling of the singular free energy depends directly on the magnetic field. Satisfyingly, in the following we shall see that the geometrical description does encode the unique features of scaling in the Griffiths model.

In view of their bearing upon the subsequent geometric analysis we also report fluctuations in magnetization and quadrupole moment on the f line $D = K + H$ for different ranges of H. For the quadrupole fluctuations we have

$$\langle (\Delta Q)^2 \rangle = 2 e^{(6H-K)\beta} \qquad (H < K/4)$$

$$= \frac{2}{5\sqrt{5}} e^{K\beta/2} \quad (H = K/4)$$

$$= \frac{1}{4} e^{K\beta/2} \qquad (H > K/4). \quad (57)$$

It is evident from the above equation that for $K/6 < H < K/4$ the divergence of quadrupole fluctuations becomes progressively weaker than that of the correlation length and eventually flattens at $H = K/6$. For $H < K/6$ the quadrupole fluctuation decays to zero on approaching zero temperature. The magnetization fluctuations follow the same pattern as the quadrupole fluctuations above except when $H < K/8$,

$$\langle (\Delta M)^2 \rangle \sim \langle (\Delta Q)^2 \rangle \quad (H > K/8)$$
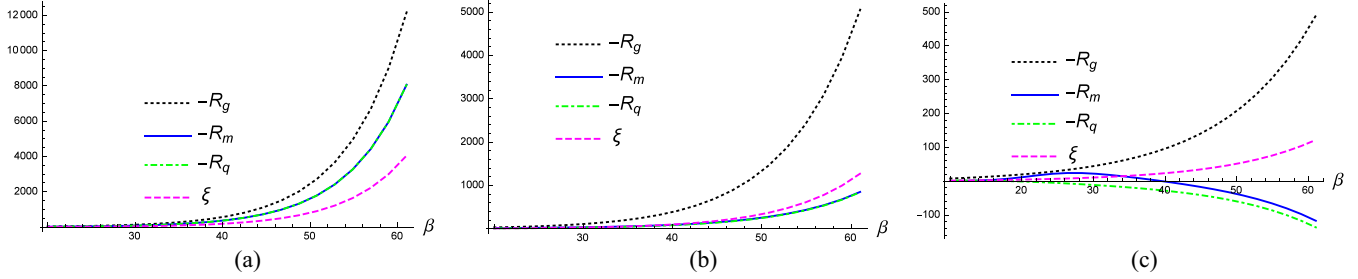
$$= 4 e^{-2H\beta} \quad (H \leqslant K/8). \quad (58)$$

FIG. 12. Temperature plots of curvatures and correlation length for the pseudocritical f line in the Griffiths model. (a) $H = 0.12, D = 0.42, K = 0.30$, (b) $H = 0.06, K = 0.30, D = 0.36$, and (c) $H = 0.04, K = 0.30, D = 0.34$.

B. Geometry of the Griffiths model

We now survey the geometry of the Griffiths model starting with the f line. For $H > K/4$ both R_m and R_q show a negative divergence and overlap with each other at low temperatures. They follow the Ruppeiner equation with $\kappa = 1$. On the other hand the three-dimensional curvature R_g follows the Ruppeiner equation with $\kappa = 3/2$. The relation with the correlation length can be worked out from Eq. (56) and is obtained as $R_m, R_q \sim 2\xi$, and $R_g \sim 3\xi$. This is shown is Fig. 12(a) where R_m and R_q are seen to completely overlap with each other. For $K/6 < H < K/4$ R_m and R_q still show a negative divergence at the same rate as the correlation length (or ψ^{-1}); however, the proportionality constant κ in the Ruppeiner equation is less than unity and steadily decreases to zero as H approaches $K/6$. For the grand curvature $R_g, \kappa = 4$ in this range. This is shown in Fig. 12(b) where the correlation length is now seen to lead the curvatures R_m and R_q, which again overlap with each other. We could say that the sectional curvatures R_m and R_q are sensitive to the same mesoscopic interactions which cause the spin and quadrupolar fluctuations to flatten as H decreases from $K/4$ to $K/6$. On the other hand the grand curvature R_g does not seem to process this information and appears to mostly respond to the magnitude of the correlation length.

Finally, for the range $H < K/6$ wherein the spin and quadrupole fluctuations decay at zero temperature, Eqs. (57) and (58), the curvatures R_m and R_q now turn positive and diverge at the same rate as the correlation length. The two curvatures, though reasonably parallel, are not as close to each

other as the previous cases. The magnitude of the proportionality constant κ now ranges from less than unity to much larger values as H approaches zero. On the other hand R_g continues to diverge to negative infinity with κ still equal to 4. This is shown in Fig. 12(c) and is favorably compared with an analogous behavior of R_q in Fig. 8 in Sec. V B. In both cases some sectional curvatures show a positive divergence at the same rate as the correlation length. While it is unusual for the state space scalar curvature to undergo a positive divergence at criticality, we believe that the same mesoscopic interaction which causes the quadratic fluctuations to decay near criticality also causes a sign change in the curvatures here.

The $H = 0$ axis does not become critical for the Griffiths model as mentioned earlier. This is reflected very well by the respective curvatures. Figure 13(a) is a representative zero-field plot with $D < K$. The curvature R_m quickly converges to a value of -1, while R_q converges to -2 and R_g to -3.5, with the correlation length decaying to zero. At the triple point $D = K$ the curvatures asymptote to $R_g \to -7.5, R_q \to -4, R_m \to -1$, and the correlation length now does not decay to zero but converges to $1/\log 2$.

For $D > K$ on the $H = 0$ axis we report a minor but interesting feature which is ably captured by the geometry of the model. As shown in Fig. 13(b) the quadratic fluctuation after initially decaying to zero undergoes a spike in fluctuation. Exactly in the middle of this spike the magnetization fluctuation sharply drops from 1 to 0. The curvature R_q remains exactly twice the correlation length as can be seen from Fig. 13(c). The curvature R_m and R_g on the other hand register their response to the correlations in magnetization by jumping to
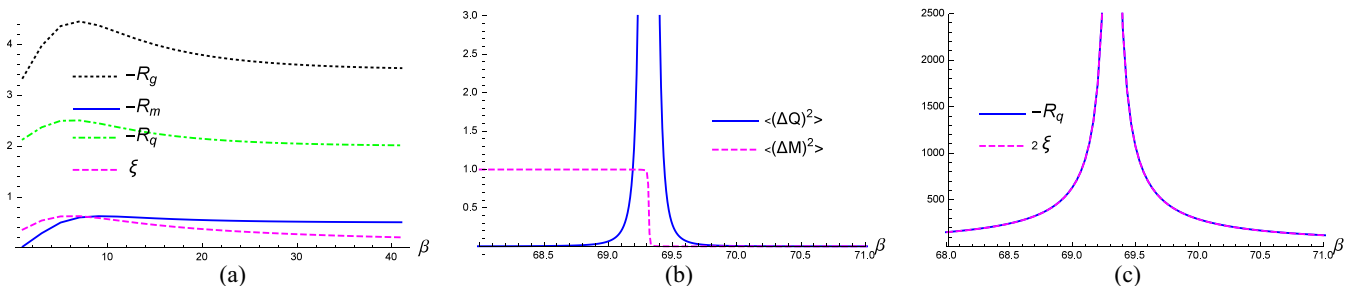

FIG. 13. (a) Scalar curvatures and correlation length for the Griiifiths model with $H = 0, K = 0.30, D = 0.31$. Plots of (b) spin and quadrupole fluctuation moments and (c) 2ξ and $-R_q$ for the same parameter values as (a).
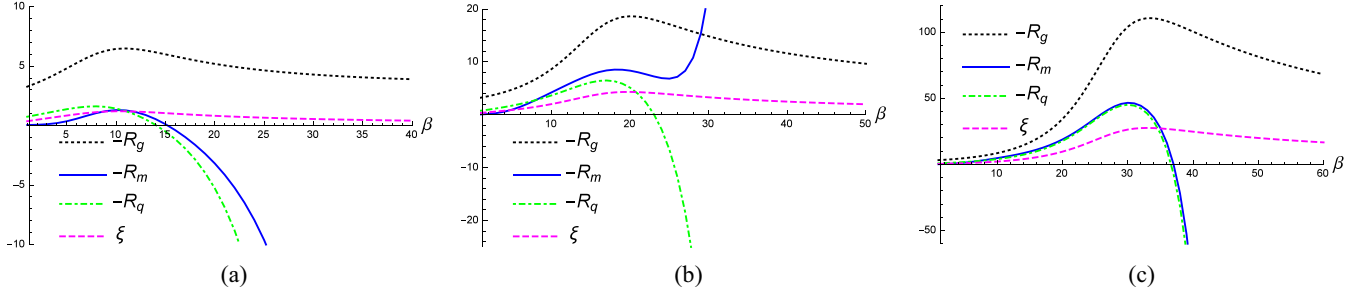
FIG. 14. Temperature plots of scalar curvatures and the correlation length for the Griffiths model. In all subfigures, $H = 0.12$, $K = 0.30$, and D values are less than but progressively closer to the f line at $D = K + H$. (a) $D = 0.36$, (b) $D = 0.41$, and (c) $D = 0.419$.

large positive values at the temperature at which the magnetization fluctuation drops to near-zero values (not shown in the figure).

We turn now to nonzero H values in regions away from the f line. In Fig. 14 we take a representative selection of plots for a fixed value of H and different values of D moving right towards the f line. In all the subfigures the curvatures R_m and R_q display a pattern reminiscent of the non-zero-field behavior in the BEG case as depicted in Fig. 11 above, perhaps reflecting a shifting nature of underlying mesoscopics, a question we hope to address in a future investigation. On the other hand the grand curvature R_g always appears to nicely track the noncritical correlation length, even if it maintains a relatively large separation with it. This again fits well with our earlier observation that for the $J = 0$ case R_g responds rather faithfully to the magnitude of the correlation length in both the critical as well as the noncritical cases.

VII. CONCLUSIONS

In this work we have undertaken a detailed analysis of the thermodynamic geometry associated with the one-dimensional BEG model and its limiting cases of the BC model and the Griffiths model. The BEG model, which is extensively used to model interacting systems with two order parameters, preserves much of the richness of its phase structure in the one-dimensional case. In addition, being exactly solvable in one dimension and with tractable expressions for the free energy and the correlation lengths, it offers an excellent opportunity to comprehensively probe its geometry.

The three-dimensional state space of the BEG model has been systematically sectioned into two relevant codimension one geometries. The associated intrinsic scalar curvatures R_q and R_m are found to be relevant to the correlations in the quadrupole and the magnetic moment, respectively. For $H = 0$ the spin and quadrupolar order parameters have separate correlation lengths ξ_1 and ξ_2, and, remarkably, it is seen that R_q and R_m encode these separately. The two sectional curvatures are seen to always follow the Ruppeiner equation near the pseudocritical lines and the pseudotricritical point, with the proportionality constant $\kappa = 1$. Making use of the Ruppeiner equation we are able to ascertain thermodynamically the full scaling forms of the singular free energy of the BEG model, thus bypassing the technically more challenging approaches employing RG analysis. The proportionality constant of the grand curvature R_g to the inverse of singular free energy,

though always of order unity, is seen to vary depending on the parameter range.

The curvatures R_g, R_m, and R_q obey the weak form of Ruppeiner's conjecture in that the trends in their variation are analogous to that of the correlation lengths even in regions far away from criticality. In much of the noncritical parameter space the decaying correlation length obtained via the transfer matrix is seen to be "enveloped" by the relevant scalar curvature. Moreover, on several occasions it has been possible to connect, albeit in a preliminary way, the sign changes or some sharp shift in the sectional curvatures to the change in the nature of M or Q fluctuations, thus suggesting a deeper connection of geometry with the nature of underlying statistical interactions.

In the Griffiths model limit, it is seen that R_g remains sensitive only to the magnitude of the correlation length in noncritical regions, while the sectional curvatures respond via changes in signature or the rate of divergence to the changing nature of statistical fluctuations. Admittedly, there are a few patches of the parameter space where we are not able explain the behavior of one or more scalar curvatures via the underlying thermodynamics.

One of the key messages in our work vis-à-vis thermodynamic geometry is that for higher dimensional parameter spaces the relevant sectional curvatures contain essential mesoscopic information not found in the full scalar curvature. Significantly, we have been able to establish that judiciously chosen sectional curvatures can encode the correlations in respective order parameters. To the best of our knowledge this is the first application to ordinary thermodynamic systems of sectional geometry induced from higher dimensional phase space, a project initiated in [35] for Kerr-Newman anti–de Sitter black holes. We hope that the approach taken here shall be gainfully employed in the study of a range of thermodynamic systems with multiple order parameters.

APPENDIX

The appendix contains detailed expressions for the scalar curvatures mentioned symbolically in subsection V A.

$$
\begin{aligned}
\mathcal{N}_1 = -2e^{-J\beta} \Big[& 37e^{2\beta J} + 4e^{16\beta J} + 5We^{\beta J} + (6W + 24)e^{15\beta J} \\
& + (24W + 334)e^{14\beta J} + (37W + 74)e^{3\beta J} + (54W + 106)e^{4\beta J} \\
& + (106W + 464)e^{5\beta J} + (274W + 980)e^{13\beta J} + (304W + 1100)e^{7\beta J} \\
& + (316W + 480)e^{6\beta J} + (396W + 1702)e^{12\beta J} + (676W + 1671)e^{8\beta J} \\
& + (703W + 1684)e^{9\beta J} + (733W + 1868)e^{11\beta J} \\
& + (740W + 2589)e^{10\beta J} + 5 \Big],
\end{aligned}
$$

$$
\begin{aligned}
\mathcal{D}_1 = W[& 6e^{2\beta J} + 2e^{7\beta J} + 2We^{\beta J} + We^{6\beta J} \\
& + (4W + 27)e^{5\beta J} + (5W + 4)e^{4\beta J} + (6W + 13)e^{3\beta J} + 2]^2,
\end{aligned}
$$

$$
W = \sqrt{e^{-2\beta J} + 8e^{\beta J}}; \tag{A1}
$$

$$
\mathcal{N}_2 = \mathcal{A}\mathcal{B},
$$

$$
\begin{aligned}
\mathcal{A} = -2e^{-\beta J} \Big[& e^{3\beta D} + (W + 6)e^{\beta(D+2J)} + 3(W + 2)e^{\beta D} \\
& + (W + 6)e^{2\beta D} + e^{6\beta J} + (W + 3)e^{4\beta J} + (2W + 3)e^{2\beta J} + W + 1 \Big],
\end{aligned}
$$

$$
\begin{aligned}
\mathcal{B} = {} & 6e^{\beta(5D+J)} + e^{\beta(D+9J)} + 4e^{4\beta D+3\beta J} + e^{3\beta D+5\beta J} \\
& + 3e^{2\beta D+7\beta J} + 14(W + 2)e^{\beta(D+3J)} + 10(W + 3)e^{\beta(D+5J)} \\
& + 5(W + 5)e^{2\beta D+5\beta J} + 2(W + 6)e^{\beta(D+7J)} + (6W + 9)e^{\beta(D+J)} \\
& + (6W + 28)e^{\beta(4D+J)}(6W + 34)e^{3\beta(D+J)} + (13W + 27)e^{\beta(2D+J)} \\
& + (14W + 41)e^{\beta(3D+J)} + (18W + 49)e^{2\beta D+3\beta J} + e^{11\beta J} \\
& + (W + 1)e^{\beta J} + (W + 5)e^{9\beta J} + 2(2W + 5)e^{7\beta J} + 2(3W + 5)e^{5\beta J} \\
& + (4W + 5)e^{3\beta J},
\end{aligned}
$$

$$
\begin{aligned}
\mathcal{D}_2 = W \big(& e^{\beta D} + e^{2\beta J} + W + 1 \big) \Big[2e^{3\beta D} + e^{2\beta(D+J)} + (W + 6)e^{\beta(D+2J)} \\
& + 3(W + 2)e^{\beta D} + (2W + 7)e^{2\beta D} + e^{6\beta J} + (W + 3)e^{4\beta J} \\
& + (2W + 3)e^{2\beta J} + W + 1 \Big]^2,
\end{aligned}
$$

$$
W = \sqrt{6e^{\beta D} + e^{2\beta D} - 2e^{\beta(D+2J)} + 2e^{2\beta J} + e^{4\beta J} + 1}. \tag{A2}
$$

---

[1] G. Ruppeiner, Rev. Mod. Phys. **67**, 605 (1995); **68**, 313 (1996).

[2] G. Ruppeiner, Phys. Rev. A **20**, 1608 (1979).

[3] R. K. Pathria and P. D. Beale, *Statistical Mechanics*, 3rd ed. (Butterworth Heinemann, Oxford, 2011).

[4] G. Ruppeiner, Phys. Rev. A **44**, 3583 (1991).

[5] G. Ruppeiner, Phys. Lett. A **383**, 703 (2019).

[6] G. Ruppeiner, A. Sahay, T. Sarkar, and G. Sengupta, Phys. Rev. E **86**, 052103 (2012).

[7] H. O. May and P. Mausbach, Phys. Rev. E **85**, 031201 (2012).

[8] A. Dey, P. Roy, and T. Sarkar, Physica A **392**, 6341 (2013).

[9] G. Ruppeiner, P. Mausbach, and H. May, Phys. Lett. A **379**, 646 (2015).

[10] G. Ruppeiner, Phys. Rev. E **86**, 021130 (2012).

[11] H. O. May, P. Mausbach, and G. Ruppeiner, Phys. Rev. E **88**, 032123 (2013).

[12] B. Mirza and H. Mohammadzadeh, Phys. Rev. E **82**, 031137 (2010).

[13] B. Mirza and H. Mohammadzadeh, Phys. Rev. E **78**, 021127 (2008).

[14] B. Mirza and H. Mohammadzadeh, Phys. Rev. E **80**, 011132 (2009).

[15] P. Castorina, D. Lanteri, and M. Ruggieri, Phys. Rev. D **102**, 116022 (2020).

[16] G. Ruppeiner and A. Seftas, Entropy **22**, 1208 (2020).

[17] G. Ruppeiner, Phys. Rev. E **57**, 5135 (1998).

[18] R. Erdem, Acta Phys. Pol. B **49**, 10 (2018).

[19] G. Ruppeiner, Phys. Rev. A **24**, 488 (1981).

[20] H. Janyszek and R. Mrugala, Phys. Rev. A **39**, 6515 (1989).

[21] B. Dolan, Proc. R. Soc. London A **454**, 2655 (1998).

[22] W. Janke, D. A. Johnston, and R. P. K. C. Malmini, Phys. Rev. E **66**, 056119 (2002).

[23] W. Janke, D. A. Johnston, and R. Kenna, Phys. Rev. E **67**, 046106 (2003).

[24] B. Dolan, D. Johnston, and R. Kenna, J. Phys. A: Math. Gen. **35**, 9025 (2002).

[25] G. Ruppeiner and S. Bellucci, Phys. Rev. E **91**, 012116 (2015).

[26] M. Blume, V. J. Emery, and R. B. Griffiths, Phys. Rev. A **4**, 1071 (1971).

[27] J. Lajzerowicz and J. Sivardière, Phys. Rev. A **11**, 2079 (1975).

[28] J. Bernasconi and F. Rys, Phys. Rev. B **4**, 3045 (1971).

[29] M. Schick and W.-H. Shih, Phys. Rev. B **34**, 1797 (1986).

[30] M. Blume, Phys. Rev. **141**, 517 (1966).

[31] H. W. Capel, Physica **32**, 966 (1966).

[32] R. B. Griffiths, Physica **33**, 689 (1967).

[33] R. Sanwari and A. Sahay, Phys. Rev. E **105**, 034135 (2022).

[34] S. Krinsky and D. Furman, Phys. Rev. B **11**, 2602 (1975).

[35] A. Sahay, Phys. Rev. D **95**, 064002 (2017).

[36] G. Ruppeiner, Phys. Rev. D **75**, 024037 (2007).

[37] A. Sahay, T. Sarkar, and G. Sengupta, J. High Energy Phys. 04 (2010) 118.

[38] S. A. H. Mansoori, B. Mirza, and E. Sharifian, Phys. Lett. B **759**, 298 (2016).

[39] E. Poisson, *A Relativist's Toolkit: The Mathematics of Black-Hole Mechanics* (Cambridge University Press, Cambridge, 2007).

[40] I. D. Lawrie and S. Sarbach, Theory of tricritical points, in *Phase Transitions and Critical Phenomena*, edited by C. Domb and J. L. Lebowitz (Academic Press, London 1984), Vol. 9.